Materials Advances

ROYAL SOCIETY OF CHEMISTRY

PAPER

View Article Online
View Journal | View Issue

Cite this: *Mater. Adv.*, 2026, 7, 3567

Atomistic origins of viscoelasticity and β-relaxation in $Cu_{64}Zr_{36}$ metallic glass and nanoglass

Param Punj Singh,[a] Dhyanesh Baskaran,[a] Omar Adjaoud,[b] Karsten Albe [b] and Raghavan Ranganathan *[a]

Received 12th December 2025,
Accepted 19th February 2026

DOI: 10.1039/d5ma01457c

rsc.li/materials-advances

Understanding the structure–property relationships in glasses is challenging due to their inherent structural disorder and non-equilibrium nature. Among these, secondary (β) relaxation plays a vital role in dictating mechanical behavior, yet its structural origins remain elusive. In this study, we employ molecular dynamics simulations to investigate the temperature-dependent viscoelastic properties of $Cu_{64}Zr_{36}$ in both metallic glass and nanoglass forms. Our results demonstrate that nanoglasses exhibit pronounced β relaxation, manifested as an additional wing near the α peak. String-like atomic motions indicative of β relaxation are prominent in nanoglass, but largely suppressed in metallic glass despite observed correlated displacements. Analysis of local short-range icosahedral and polyheral motifs shows that regions with reduced structural order correspond to greater energy dissipation. These findings provide new atomistic insights into the microscopic mechanisms governing β relaxation and their implications for the mechanical performance of metallic glasses.

1. Introduction

Nanoglasses (NGs) are a class of materials synthesized by consolidating nanoscale clusters of amorphous glass, resulting in a structure characterized by a central amorphous region separated by glass–glass interphases.[1–3] The glass–glass interfaces formed during compaction exhibit an increased free volume and compositional heterogeneity compared to the interior glass regions, which has been attributed to surface segregation occurring before compaction.[4–6] Therefore, microstructural changes within the NG can be utilized to adjust the interfacial structure, allowing efficient optimization of the mechanical properties of the NGs.[1,7–10]

Metallic glasses, similar to other glassy materials, demonstrate a wide range of viscoelastic and relaxation behaviors, which are characterized by structural changes at the molecular and atomic scales in a broad spectrum of temperatures and frequencies.[11–13] In glasses, relaxation processes are traditionally categorized into two main types: the primary (α) relaxation, which arises from large-scale irreversible atomic rearrangements responsible for the glass transition, and the Johari–Goldstein secondary (β) relaxation,[14,15] which is attributed to localized atomic rearrangements.

Recent molecular dynamics (MD) simulations have demonstrated that, in metallic glasses, β relaxations are facilitated by atomic motions characterized by string-like cooperative atomic rearrangements within the slow-moving matrix.[15–17] In Dynamic Mechanical Spectroscopy (DMS), the β relaxations observed in the loss modulus plots can manifest in various forms. They may appear as well-defined peaks in certain glassy materials, as excess wings extending from the tail of the α relaxation, or, in some cases, they may be completely absent.[18–20]

Numerous studies have demonstrated that β relaxations in metallic glasses are primarily governed by the local atomic order, which is influenced by both physical treatments and chemical composition, as evidenced by diffraction techniques such as neutron and X-ray scattering experiments.[21] The local atomic configuration defining the icosahedral structures forms the fundamental building blocks of metallic glasses, with atoms within these structures exhibiting rigid local structure, high shear resistance, and slower relaxation.[22,23] The structural inhomogeneities inherent to these materials give rise to damping effects associated with structural relaxation, commonly referred to as anelastic relaxation, which can be understood as a form of viscoelastic damping.[14–26] These damping responses occur due to the out-of-phase nature of stress and strain during DMS deformation cycles that are highly temperature and frequency-dependent.[27,28] Therefore, a comprehensive

[a] *Department of Materials Engineering, Indian Institute of Technology Gandhinagar, Gandhinagar, 382355, Gujarat, India. E-mail: rraghav@iitgn.ac.in*
[b] *Institute of Materials Science, Technische Universitat Darmstadt, Otto-Berndt-Str.3, 64287, Darmstadt, Germany*

understanding of viscoelastic behavior is essential for elucidating the relaxation and mechanical properties of NGs, as these aspects are closely interconnected.

2. Computational methodology

In this work, we investigate the distinct viscoelastic behavior and underlying relaxation mechanisms of $Cu_{64}Zr_{36}$ metallic glass (MG) and nanoglass (NG) using MD simulations. All simulations were performed with the Large-scale Atomic/Molecular Massively Parallel Simulator (LAMMPS) package.[29] Visualization of the atomic structure and the atomic-scale deformation mechanisms was done using the OVITO software.[30] The atomistic model of $Cu_{64}Zr_{36}$ MG and NG were prepared following the methodology detailed in our previous studies.[31–33] The interatomic interactions were described by the embedded atom method (EAM) potential developed for $Cu_{64}Zr_{36}$.[34] MG was prepared by quenching an equilibrated melt at a temperature of 2000 K to 50 K with a cooling rate of 0.01 K ps^{-1}. The $Cu_{64}Zr_{36}$ MG model prepared demonstrates properties consistent with previous studies.[35–38] The NG structure was prepared in accordance with our previous work.[31] The NG was formed by carving out glassy spheres from $Cu_{64}Zr_{36}$ MG model, later consolidating polydisperse glassy spheres to form the NG consisting of inner-glassy spheres of diameter about 7 nm separated by glass–glass interface. The consolidation process was carried out at approximately 50 K, during which an external hydrostatic pressure of 5 GPa was applied and subsequently released to 0. During consolidation, the interfaces and glassy regions of the nanoglass can be primarily distinguished by the presence of highly sheared and lightly sheared atoms, respectively. Shear strain analysis was used to identify interfacial atoms that experienced significant shear deformation ($\eta > 0.2$) throughout the consolidation process.[31] The resulting bulk and the nanoglass have a size of about 18 nm × 18 nm × 18 nm, containing about 364 500 atoms. Model structures from the resulting protocol are shown for the $Cu_{64}Zr_{36}$ MG and the NG in Fig. 1(a) and (b). For all the MD simulations in this study, we used periodic boundary conditions and a timestep of 2 fs. The Nosé–Hoover thermostat and barostat, as implemented in LAMMPS, were used to control temperature and pressure.

3. Results and discussion

Fig. 1c presents the radial distribution function $g(r)$ of MG and NG for varying temperature. The $g(r)$ plots exhibit a pronounced first peak in both the MG and NG systems at r = 2.75 Å, reflecting the chemical short-range order in Cu–Zr. The second peak shows a characteristic splitting, which is indicative of the glassy structure in MG and NG, respectively. For both systems, it is evident that short-range order persists even as the temperature increases. However, beyond glass transition temperature (T_g) close to 800–840 K, the secondary peaks in the RDF merge to form a broad hump. The $g(r)$ results are consistent with previous theoretical and experimental studies on $Cu_{64}Zr_{36}$ MGs.[39,40] The shear stress–strain response is shown in Fig. 1d. It is important to note that the $g(r)$ and shear stress–strain plots are included here because they provide key parameters for performing viscoelastic simulations and for understanding the molecular response during relaxation. The simple shear simulation was performed at a strain rate of 1.0×10^8 s^{-1} and a temperature of 50 K. To check for potential anisotropy, the shear deformation was applied along all three principal shear directions (here, denoted by the tilt factors, *xy, xz, and yz*). Notably, for both MG and NG, the shear stress–strain responses are identical across all directions, indicating the isotropic nature of the atomic models. However, the MG exhibits a higher Young's modulus and twice the shear strength in comparison to the NG in all shear directions. For the subsequent linear viscoelastic simulations, an elastic strain of ε = 0.0167, as marked in Fig. 1d, is selected as the strain for the oscillatory shear simulations.

To investigate the temperature-dependent viscoelastic properties, a non-equilibrium oscillatory shear deformation was applied,[27,41–43] and the resulting shear stress was analyzed. The equations of motion were integrated according to the SLLOD algorithm,[44,45] equivalent to the Lees–Edwards 'sliding brick' boundary conditions. The shear strain during oscillatory shear deformation was determined by a sinusoidal function, which can be expressed as

$$\gamma_{xy} = \gamma_0 \sin(\omega t) \quad (1)$$

where γ_{xy} is the oscillatory shear amplitude and ω is the angular frequency. The virial shear stress,[46] which is also a sinusoidal function, can be expressed as

$$\tau_{xy} = \tau_0 \sin(\omega t + \delta) \quad (2)$$

where τ_0 is the shear stress amplitude, and δ is the phase shift between the stress and the strain profile. The storage (G'), loss (G'') moduli, and loss tangent ($\tan\delta$) are calculated as

$$G' = \frac{\tau_0 \cos(\delta)}{\gamma_0} \quad G'' = \frac{\tau_0 \sin(\delta)}{\gamma_0} \quad \tan\delta = \frac{G''}{G'} \quad (3)$$

It is well known that the relaxation and damping in glasses are functions of temperature and frequency of deformation.[27] As we are primarily interested in understanding temperature-dependent relaxation processes, we use two oscillatory shear frequencies corresponding to time periods of 0.1 and 1 ns. For each shear frequency, a temperature-sweep simulation was conducted spanning 120 K to 1000 K for a total simulation time of 20 ns. The virial shear stress and τ_{xy} were measured at intervals of every 0.1 ps, and the stress response was averaged over the last 20 cycles to determine the viscoelastic behavior.

Fig. 2 illustrates the temperature-dependent G' and G'' moduli of MG and NG for the two shear frequencies. Fig. 2(a) and (b) compares the G' of MG and NG, respectively. For both models, it is evident that at shorter oscillation periods (higher frequencies), G' is higher compared to lower frequencies, as atoms have less time to respond to the applied deformation.

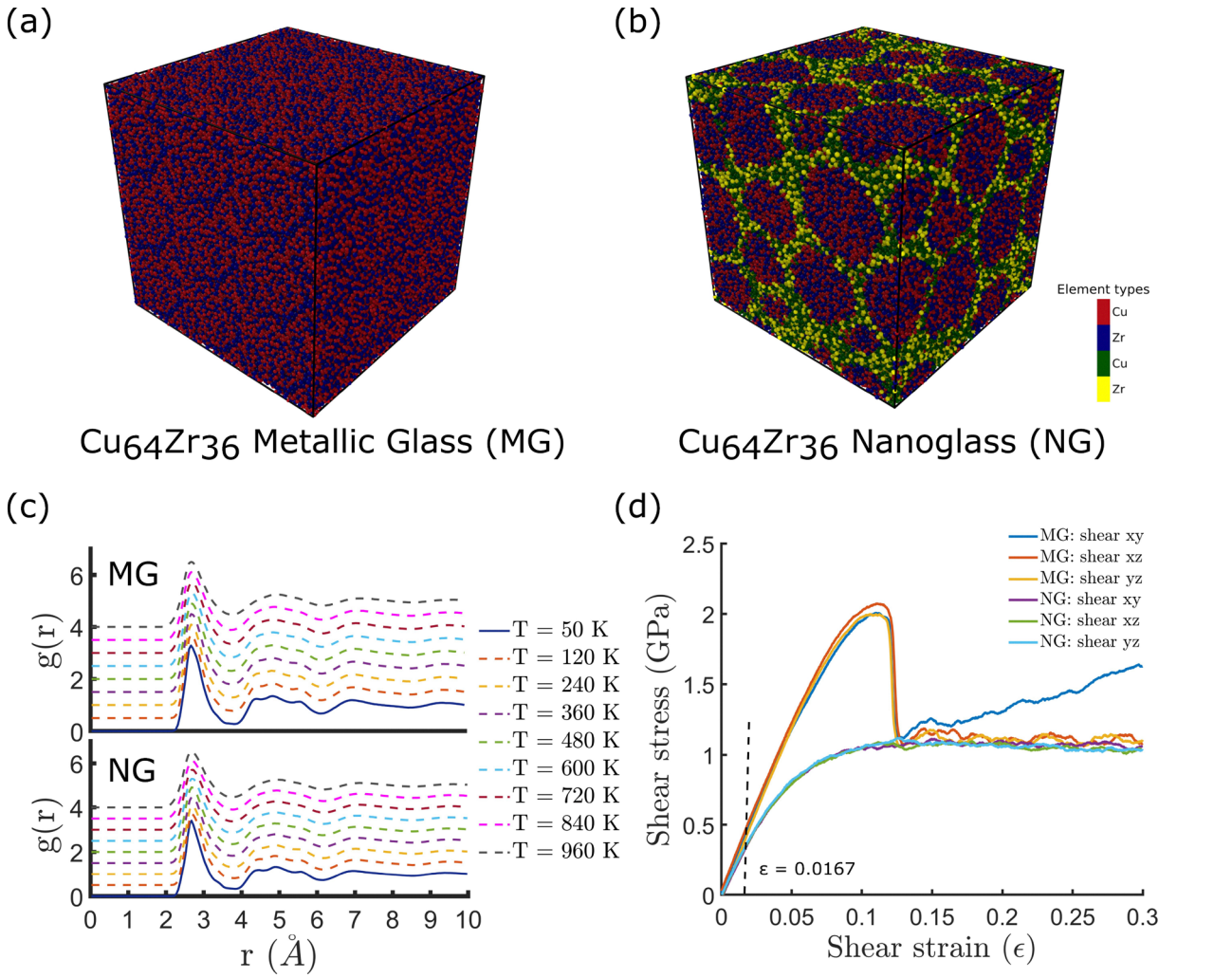

Fig. 1 Equilibrated snapshots of atomic configurations of a $Cu_{64}Zr_{36}$ (a) metallic glass (MG) and (b) nanoglass (NG). Red and blue atoms are Cu and Zr atoms in the glass phase; green and yellow atoms are Cu and Zr atoms at the interface in $Cu_{64}Zr_{36}$ nanoglass. (c) Radial distribution function $g(r)$ of MG and NG at varying temperature; curves are shifted for clarity. (d) Shear stress–strain curves of MG and NG for all three shear directions on independent shear planes (denoted by the tilt factors, *xy*, *yz*, and *zx*).

At higher frequencies, the material exhibits more elastic, solid-like behavior than at lower frequencies. Additionally, a transition in G' is observed near the onset of T_g, which shifts to higher temperatures with increasing frequency, similar to other amorphous materials.[47,48] Compared to NG, the G' of MG is higher at all shear frequencies, consistent with the higher shear modulus and shear strength of MG observed in the simple shear simulations, as shown in Fig. 1d.

While G' characterizes the non-dissipative elastic response, G'' provides insight into the material's energy dissipation under oscillatory shear. Fig. 2(c) and (d) compares the G'' of MG and NG, respectively. It is important to note that G'' remains small at low temperatures due to limited atomic mobility. As the temperature increases, G'' rises as atomic rearrangements become more pronounced, leading to enhanced viscous flow. A peak appears near T_g corresponding to the α-relaxation, where structural relaxation dominates. Beyond T_g, the material flows more readily, and decreases G'' accordingly. However, T_α shifts to larger temperatures at higher frequencies, consistent with the G'. Despite the structural heterogeneity of the NG, no difference is observed in the temperature corresponding to the G'' peak T_α between the two structures. The T_α values were determined to be 760 K and 880 K for oscillation periods of 1 ns and 0.1 ns, respectively. But across the entire temperature range shown here, NG exhibits higher G'' than MG at equivalent shear frequencies. However, the G'' in NG exhibits a distinctive shoulder-like feature in the temperature range of 400–740 K, commonly referred to as 'excess wings', which correspond to β-relaxations, as evident in Fig. 2d. Of particular importance is the difference in β-relaxations observed in NG, which arises from its structural heterogeneity. The excess volume and the absence of structurally stable short-range motifs, such as icosahedral clusters at the glass–glass interface, enhance atomic mobility, resulting in greater stress dissipation even at intermediate and low temperatures. Fig. S1, supplementary material, shows the evolution of potential energy over 20 cycles

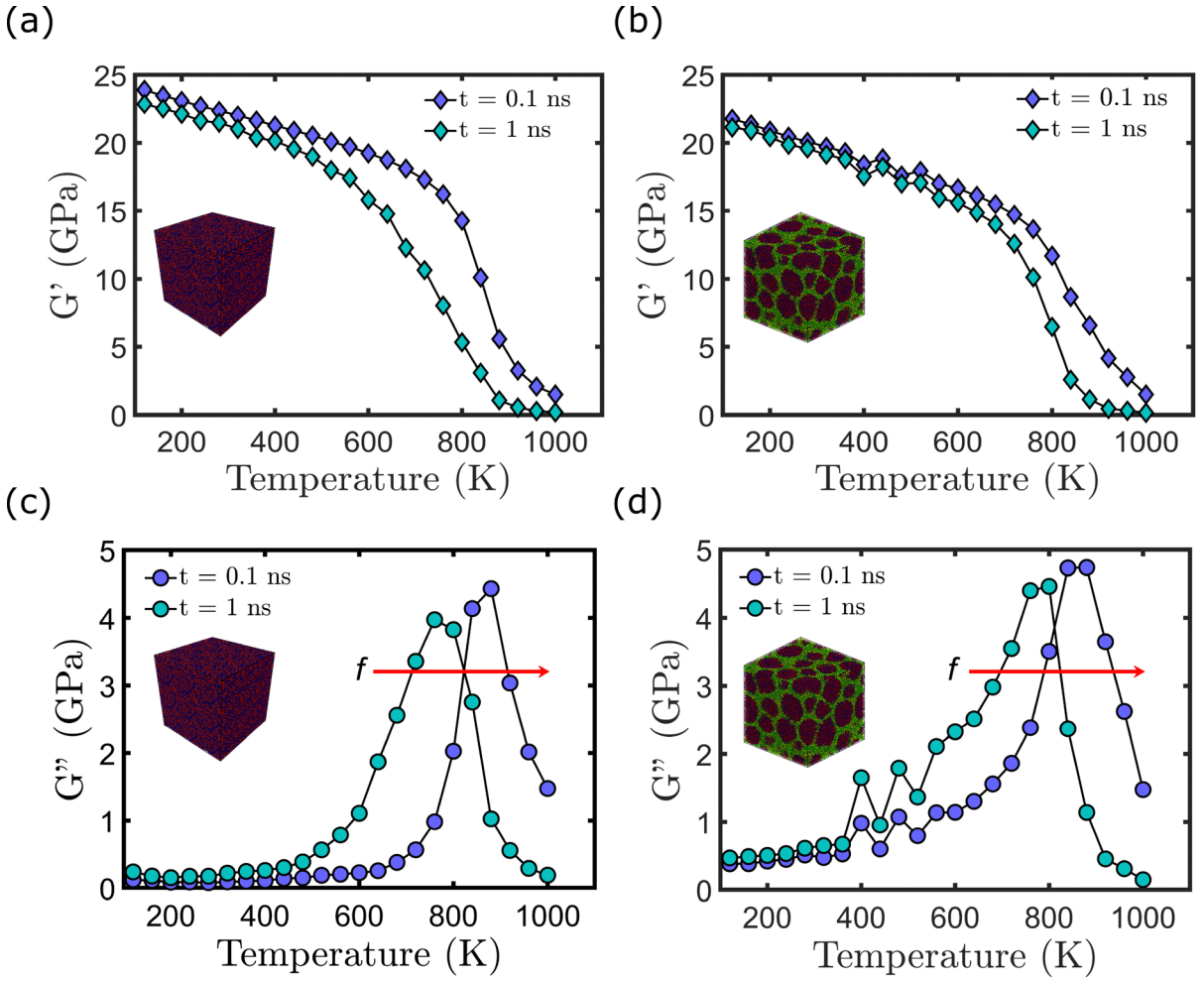

Fig. 2 (a) and (b) Storage modulus (G') and (c) and (d) loss modulus (G'') of $Cu_{64}Zr_{36}$ MG and NG for shear oscillation periods of 0.1 and 1 ns.

of oscillatory deformation with a time period of 0.1 ns at 640 K, 680 K, and 720 K within the β-relaxation range. NG exhibits a monotonic decrease in potential energy at all temperatures, whereas the potential energy of MG remains nearly constant. This reduction indicates enhanced relaxation in NG, facilitating energy dissipation and enabling the system to attain a lower-energy atomic configuration during shear deformation.

To understand the atomic mechanisms underlying the relaxation behavior in MG and NG, the spatio-temporal atomic dynamics were analyzed using the intermediate scattering function (ISF) for both MG and NG at temperatures of 680 K and 880 K, respectively. The ISFs were computed using atomic trajectories recorded at a temporal interval of 0.02 ps to accurately capture particle displacements. Fig. 3 presents ISF at temperatures of 680 K and 880 K, corresponding to the presence of β- and α-relaxations, respectively, in both MG and NG. The wave vector k was varied to probe the system dynamics across different length and time scales. For instance, low k values capture long-range collective dynamics, whereas high k values focus on short-range vibrations and atomic diffusion. The plots exhibit an initial ballistic regime, followed by the cage motion of atoms (β-relaxation) at intermediate times and, subsequently, the escape of atoms from the cage, characterized by a stretched exponential behavior. The temperature dependence of the ISF is evident, as the cage motion persists for a longer duration at the lower temperature of 680 K compared to 880 K. At both 680 K and 880 K, while MG and NG share broadly similar relaxation behavior, NG demonstrates a more rapid initial relaxation phase, particularly at k = 0.8 Å. Nevertheless, the total relaxation times for both systems remain largely equivalent, as shown in Fig. 3(a) and (c). This is consistent with the G'' peaks observed at a similar temperature (*i.e.*, at T = 760 K and t = 1 ns). However, Fig. 3(b) and (d), which presents the ISF of NG, shows a separate comparison of the relaxation behavior in the grain interiors and the glass–glass interfaces. It is evident from the plots that Cu and Zr atoms at the interfaces relax faster than those in the grain interiors at 680 K and 880 K, respectively. Overall, the ISF analysis indicates that, in addition to the relaxation behavior of the glassy interiors present in both MG and NG, the interfaces in NG play a vital role in its relaxation mechanism.

The atomic mechanisms underlying the observed relaxation phenomena in MG and NG are elucidated by further analyzing atomic rearrangements during oscillatory shear simulations.

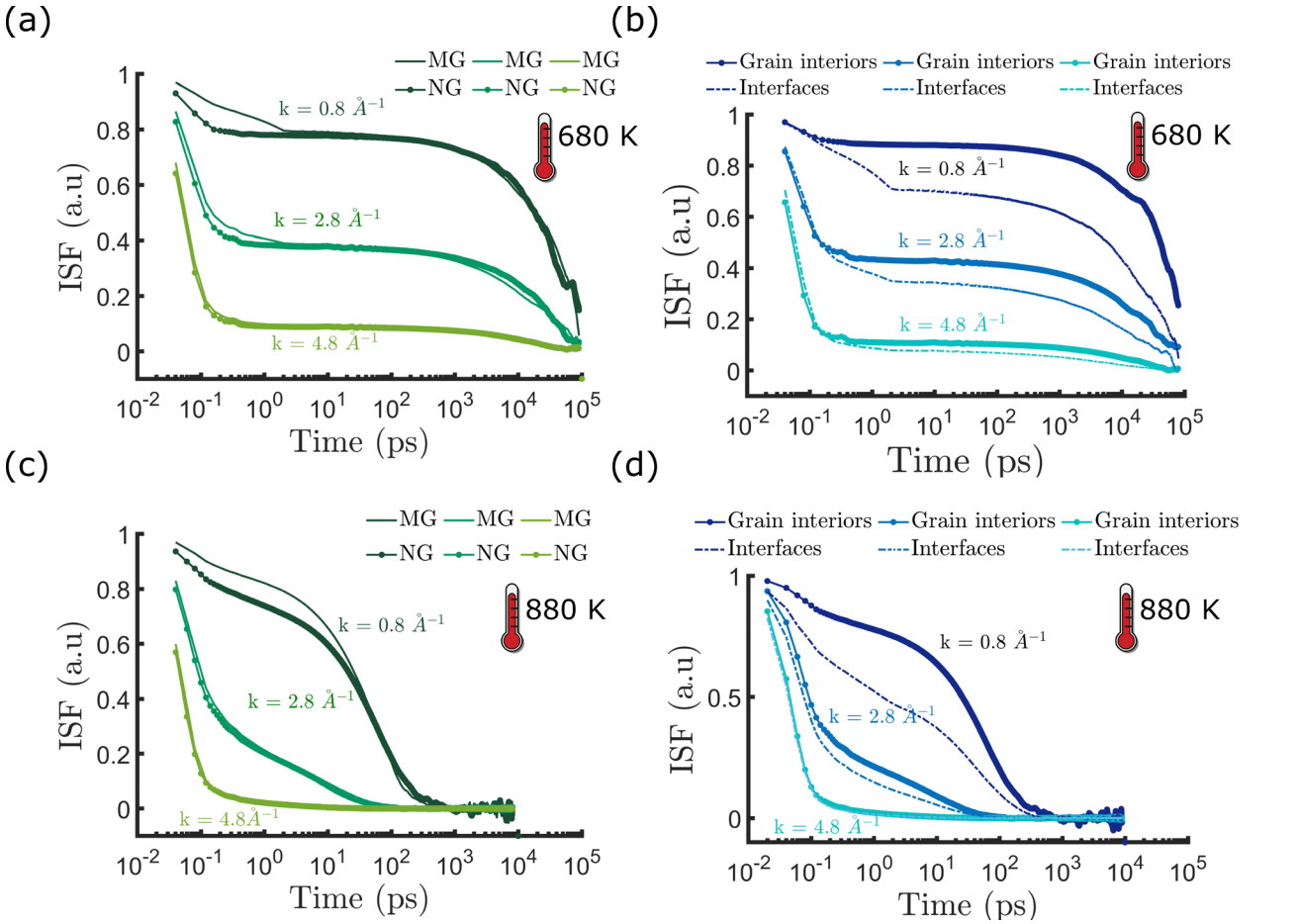

Fig. 3 Intermediate scattering function (ISF) of (a) and (c) metallic glass and nanoglass at 680 K and 880 K. (b) and (d) Comparison of the ISF between atoms in the grain interiors and at the interfaces of the nanoglass at 680 K and 880 K, respectively.

Firstly, the atomic displacements in MG and NG are considered. Fig. 4a shows the distribution of the magnitude of atomic displacements at T = 680 K, where β-relaxation is prominent in both NG and MG for an oscillatory time period of 0.1 ns. The plot reveals a noticeable peak at short displacements (≈ 1 Å) followed by a distinguishable hump for both MG and NG systems. At the range of 2–4 Å, NG dicpict a larger fraction of atomic jumps to its nearest neighbors. This position of the hump in the displacement histogram directly corresponds to the first peak in the pair distribution function $g(r)$, see Fig. 4b, which signifies the likelihood of atomic hopping to the first nearest neighbor shell. Upon analyzing the atomic displacements, it is observed that some atoms tend to move rapidly, following a cooperative string-like motion. These string-like motions in MG and NG were analyzed by computing atomic displacements relative to an initial reference configuration. A suitable cutoff distance, corresponding to the position of the first peak in the $g(r)$ plot (*i.e.*, here 2.75 Å), indicative of the typical nearest-neighbor distance, was employed to identify clusters of atoms exhibiting string-like motion. Fig. 4c highlights the string-like motion of fast-moving atoms in NG at T = 680 K, observed at the end of 20 shear cycles. The left panel in Fig. 4c shows displacement vectors, marked in red, within a 2D sliced representation of MG and NG, respectively. Interestingly, these fast-moving atoms were observed to be concentrated in the interfacial regions of the NG (see SI, Fig. S3). The right panel depicts a 3D representation of atoms, color-coded according to clusters involved in cooperative string-like motion. At 680 K (during β-relaxation), NG clearly exhibits a larger number of fast-moving atoms, resulting in more clusters participating in string-like motion. It is also noted that this phenomenon is observed exclusively in NG at the relatively lower temperature range of 400–500 K, and is absent in MG (see SI, Fig. S2). Fig. 4e, presents the histogram of string lengths (N_{string}) for MG and NG at T = 680 K. It is observed that the string lengths in $Cu_{64}Zr_{36}$ MG and NG are not significant, with the longest string comprising five atoms. Comparatively, NG contains a larger number of such atoms than MG, implying enhanced relaxation in NG, as also evidenced by the excess wing in the plot G'' plot. To further analyze the effect of structural heterogeneity in NG, the non-affine displacement (D_{min}^2)[49,50] was computed for MG and NG over the temperature range of 640–720 K. Fig. 4d, presents the probability distribution of D_{min}^2 for the systems. It is evident that the non-affine displacement in NG (shown in red) exhibits relatively larger atomic displacements, leading to more shear compared to MG

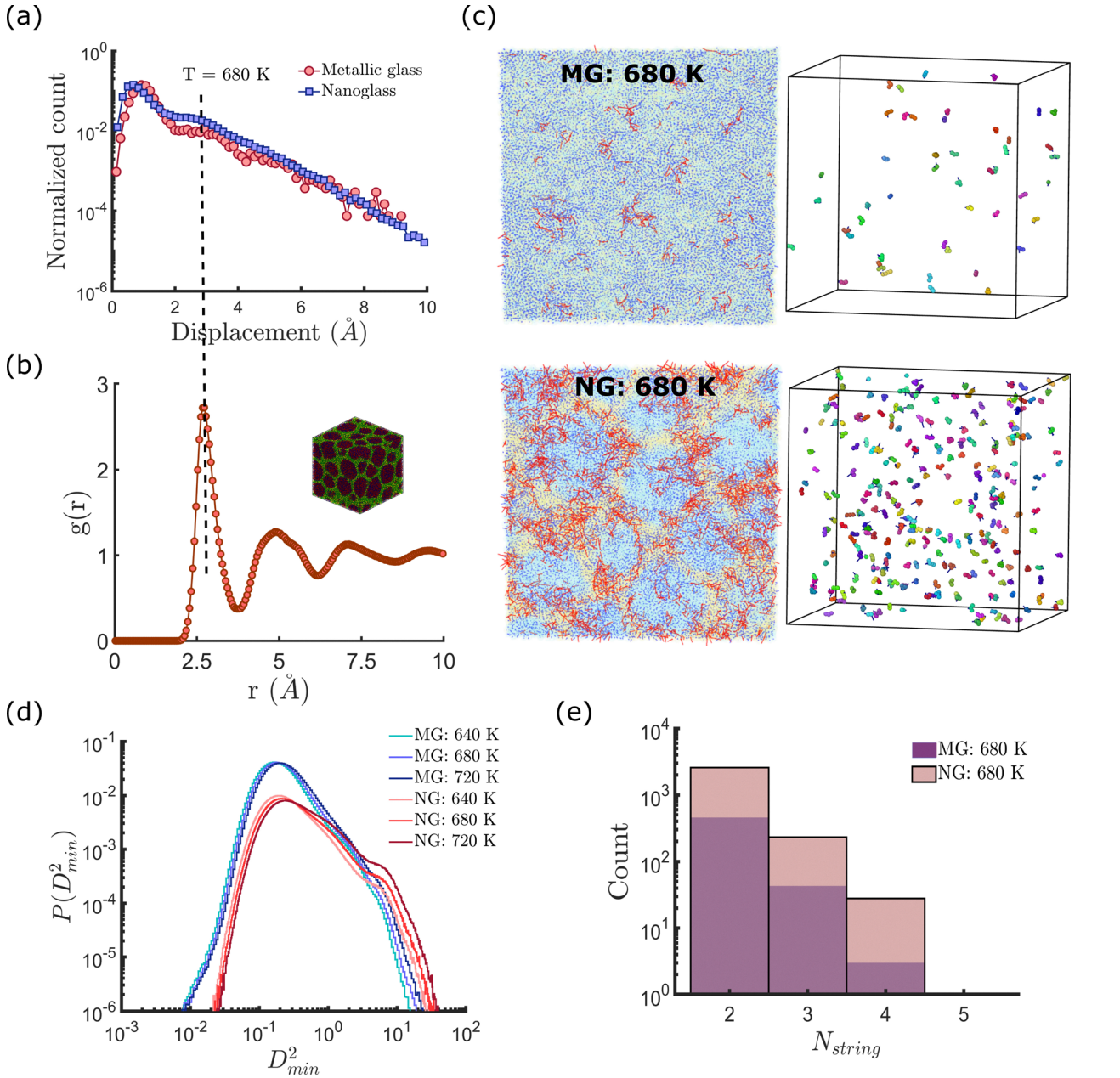

Fig. 4 (a) Distribution of atomic displacements in MG and NG at 680 K, (b) pair distribution function ($g(r)$) of NG, (c) 2D sliced MG and NG (left panel; color-coded by displacement relative to non-affine displacement, with red indicating atoms exhibiting higher displacement.) and 3D string clusters in MG and NG (right panel; color-coded according to the number of clusters.) at 680 K, (d) probability distribution of non-affine displacement (D_{min}^2) of MG and NG for varying temperature, and (e) histograms of string counts (N_{string}) in MG and NG, respectively.

(shown in blue) as a function of temperature. The contoured map of the spatial distribution of D_{min}^2 is also provided in the SI, Fig. S4, depicting more number of soft spots formed by small groups of atoms in NG that are most prone to shear transformation under oscillatory deformation.

To further understand the effect of local short-range structures on viscoelastic behavior, the evolution of the most prominent Cu-centered ($\langle 0,0,12,0\rangle$) full icosahedra and ($\langle 0,2,8,2\rangle$) polyhedra atomic configurations was analyzed by Voronoi tessellation. In $Cu_{64}Zr_{36}$ MG, the short-range structure predominantly consists of Cu-centered icosahedral clusters, whereas in NG, the presence of interfaces leads to the distortion of these full icosahedra into polyhedra, a phenomenon that has been widely studied.[31,35,40,51] These local clusters form stable atomic arrangements with a relatively high local atomic packing density. Under deformation, they contribute significantly to shear resistance by forming rigid atomic configurations. As a result, the density of Cu-centered icosahedral clusters exhibits an inverse correlation with energy dissipation.[52] Fig. 5(a) and (b) depicts the Cu-centered $\langle 0,0,12,0\rangle$ and $\langle 0,2,8,2\rangle$ fractions for both MG and NG before and after the oscillatory shear cycles. The initial fraction of these short-range structures is consistent

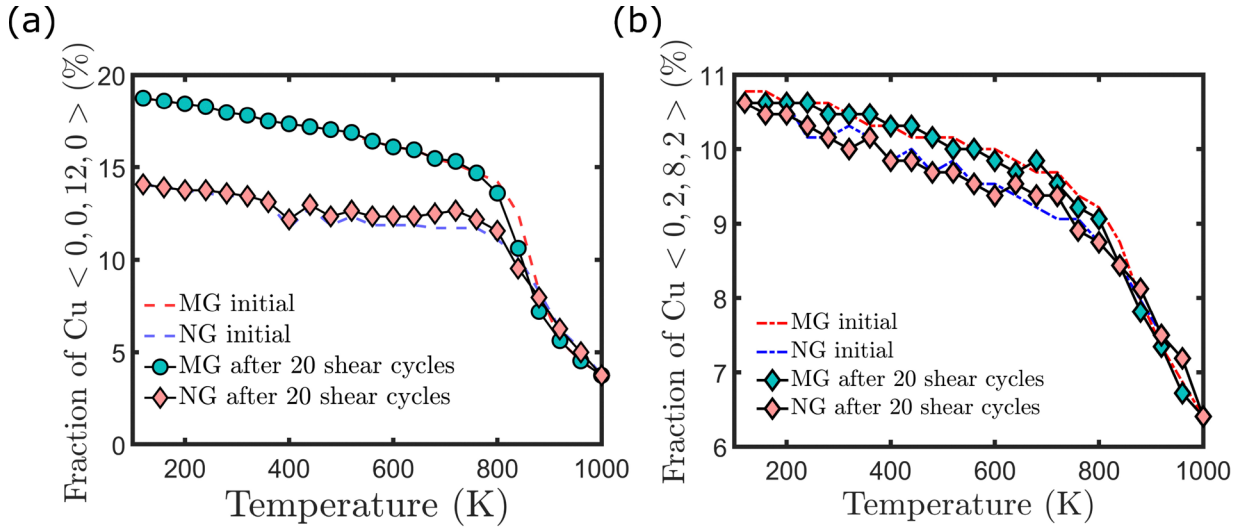

Fig. 5 (a) Fraction of Cu-centered ⟨0,0,12,0⟩ full icosahedra and (b) fraction of Cu-centered ⟨0,2,8,2⟩ polyhedra in MG and NG at the start and at the end of 20 oscillatory shear cycles.

with previous studies on $Cu_{64}Zr_{36}$ MG and NG.[31,35] In Fig. 5a, at temperatures well below the glass transition temperature, MG exhibits the highest fraction of ⟨0,0,12,0⟩ full icosahedral structures, owing to the presence of bulk amorphous regions. This is also reflected in MG having a higher G' compared to NG. This fraction gradually decreases with increasing temperature. As the system approaches the glass transition temperature, the icosahedral fractions in both MG and NG converge, as expected, due to their structural similarity in the liquid state. The lower prevalence of Cu-centered icosahedral configurations in NG is associated with enhanced energy dissipation, arising from the limited presence of rigid local atomic structures, as reflected in NG's behavior. Similarly, the ⟨0,2,8,2⟩ polyhedra fraction with respect to temperature is analyzed in Fig. 5b. A similar fraction of ⟨0,2,8,2⟩ polyhedra in MG and NG arises from their energetically favorable dominant local structure. As a function of temperature, the polyhedra exhibit a trend similar to that of Cu-centered full icosahedra, with their fraction gradually decreasing until a pronounced change occurs near T_g.

4. Conclusions

In conclusion, all-atom molecular dynamics simulations reveal a correlation between viscoelastic properties and relaxation behavior of MG and NG, linking these phenomena to their structural characteristics. The pronounced extra wing in the loss moduli of NG is directly associated with prominent string-like atomic motion observed in NG, as also evidenced from the intermediate scattering functions. Furthermore, variations in the fraction of ⟨0,0,12,0⟩ icosahedra and ⟨0,2,8,2⟩ polyhedra are consistent with the presence of β-relaxations, highlighting the structural origins of their distinct damping and relaxation responses.

Conflicts of interest

There are no conflicts to declare.

Data availability

The data supporting this article have been included as part of the supplementary information (SI): evolution of potential energy during oscillatory shear simulations at temperatures characteristic of the β-relaxation regime, the formation of string-like atomic clusters in nanoglasses at lower temperatures (400–480 K), and the associated atomic displacements under oscillatory shear, including the characterization of non-affine displacement fields. See DOI: https://doi.org/10.1039/d5ma01457c.

Acknowledgements

The authors acknowledge the Param Ananta supercomputing facility at IIT Gandhinagar for the simulations reported in this work.

References

1 J. Jing, A. Krämer, R. Birringer, H. Gleiter and U. Gonser, Modified atomic structure in a Pd Fe Si nanoglass: A Mössbauer study, *J. Non-Cryst. Solids*, 1989, **113**, 167–170.
2 H. Gleiter, Nanoglasses: a new kind of noncrystalline materials, *Beilstein J. Nanotechnol.*, 2013, **4**, 517–533.
3 Y. Ivanisenko, C. Kübel, S. H. Nandam, C. Wang, X. Mu, O. Adjaoud, K. Albe and H. Hahn, Structure and properties of nanoglasses, *Adv. Eng. Mater.*, 2018, **20**, 1800404.
4 O. Adjaoud and K. Albe, Interfaces and interphases in nanoglasses: Surface segregation effects and their implications on structural properties, *Acta Mater.*, 2016, **113**, 284–292.

5 C. Wang, D. Wang, X. Mu, S. Goel, T. Feng, Y. Ivanisenko, H. Hahn and H. Gleiter, Surface segregation of primary glassy nanoparticles of $Fe_{90}Sc_{10}$nanoglass, *Mater. Lett.*, 2016, **181**, 248–252.
6 J. Fang, U. Vainio, W. Puff, R. Wurschum, X. Wang, D. Wang, M. Ghafari, F. Jiang, J. Sun and H. Hahn, *et al.*, Atomic structure and structural stability of $Sc_{75}Fe_{25}$ nanoglasses, *Nano Lett.*, 2012, **12**, 458–463.
7 H. Gleiter, Our thoughts are ours, their ends none of our own: are there ways to synthesize materials beyond the limitations of today?, *Acta Mater.*, 2008, **56**, 5875–5893.
8 X. L. Wang, F. Jiang, H. Hahn, J. Li, H. Gleiter, J. Sun and J. X. Fang, Plasticity of a scandium-based nanoglass, *Scr. Mater.*, 2015, **98**, 40–43.
9 M. Zhang, Q.-M. Li, J.-C. Zhang, G.-P. Zheng and X.-Y. Wang, The prominent combina tion of ultrahigh strength and superior tensile plasticity in Cu–Zr nanoglass connected by oxide interfaces: A molecular dynamics study, *J. Alloys Compd.*, 2019, **801**, 318–326.
10 K. Albe, Y. Ritter and D. Şopu, Enhancing the plasticity of metallic glasses: Shear band formation, nanocomposites and nanoglasses investigated by molecular dynamics simulations, *Mech. Mater.*, 2013, **67**, 94–103.
11 Q. Yang, C.-Q. Pei, H.-B. Yu and T. Feng, Metallic nanoglasses with promoted β-relaxation and tensile plasticity, *Nano Lett.*, 2021, **21**, 6051–6056.
12 H. Yu, X. Shen, Z. Wang, L. Gu, W. Wang and H. Bai, Tensile plasticity in metallicglasses with pronounced β relaxations, *Phys. Rev. Lett.*, 2012, **108**, 015504.
13 H. Voigt, A. Rigoni, E. Boltynjuk, H. Rösner, H. Hahn and G. Wilde, In situ TEM studies of relaxation dynamics and crystal nucleation in thin film nanoglasses, *Mater. Res. Lett.*, 2023, **11**, 1022–1030.
14 H.-B. Yu, R. Richert and K. Samwer, Structural rearrangements governing Johari-Goldstein relaxations in metallic glasses, *Sci. Adv.*, 2017, **3**, e1701577.
15 H.-B. Yu, M.-H. Yang, Y. Sun, F. Zhang, J.-B. Liu, C.-Z. Wang, K.-M. Ho, R. Richert and K. Samwer, Fundamental link between β relaxation, excess wings, and cage-breaking in metallic glasses, *J. Phys. Chem. Lett.*, 2018, **9**, 5877–5883.
16 G. P. Johari and M. Goldstein, Viscous liquids and the glass transition. III. Secondary relaxations in aliphatic alcohols and other nonrigid molecules, *J. Chem. Phys.*, 1971, **55**, 4245–4252.
17 G. R. Arumugam Kumar, K. Arora, M. Aggarwal, S. Swayamjyoti, P. P. Singh, K. K. Sahu and R. Ranganathan, Structure–property predictions in metallic glasses: In sights from data-driven atomistic simulations, *J. Mater. Res.*, 2025, **40**, 36–68.
18 C. Gainaru, R. Kahlau, E. A. Rössler and R. Böhmer, Evolution of excess wing and β-process in simple glass formers, *J. Chem. Phys.*, 2009, **131**, 184510.
19 Z. Zhao, P. Wen, C. Shek and W. Wang, Measurements of slow β-relaxations in metallic glasses and supercooled liquids, *Phys. Rev. B: Condens. Matter Mater. Phys.*, 2007, **75**, 174201.
20 P. Rösner, K. Samwer and P. Lunkenheimer, Indications for an ''excess wing'' in metallic glasses from the mechanical loss modulus in $Zr_{65}Al_{7.5}Cu_{27.5}$, *Europhys. Lett.*, 2004, **68**, 226.
21 Z.-Y. Zhou, Q. Yang and H.-B. Yu, Toward atomic-scale understanding of structure305 dynamics-properties relations for metallic glasses, *Prog. Mater. Sci.*, 2024, 101311.
22 Y. Cheng and E. Ma, Atomic-level structure and structure–property relationship in metallic glasses, *Prog. Mater. Sci.*, 2011, **56**, 379–473.
23 B. Ruta, E. Pineda and Z. Evenson, Relaxation processes and physical aging in metallic glasses, *J. Phys.: Condens. Matter*, 2017, **29**, 503002.
24 W. Dmowski, T. Iwashita, C.-P. Chuang, J. Almer and T. Egami, Elastic heterogeneity in metallic glasses, *Phys. Rev. Lett.*, 2010, **105**, 205502.
25 L. Huo, J. Zeng, W. Wang, C. T. Liu and Y. Yang, The dependence of shear modulus on dynamic relaxation and evolution of local structural heterogeneity in a metallic glass, *Acta Mater.*, 2013, **61**, 4329–4338.
26 N. Morito and T. Egami, Internal friction and reversible structural relaxation in the metallic glass $Fe_{32}Ni_{36}Cr_{14}P_{12}B_6$, *Acta Metall.*, 1984, **32**, 603–613.
27 R. Ranganathan, Y. Shi and P. Keblinski, Commonalities in frequency-dependent vis coelastic damping in glasses in the MHz to THz regime, *J. Appl. Phys.*, 2017, **122**, 145103.
28 R. Lakes and J. Quackenbush, Viscoelastic behaviour in indium-tin alloys over a wide range of frequencies and times, *Philos. Mag. Lett.*, 1996, **74**, 227–232.
29 S. Plimpton, Fast parallel algorithms for short-range molecular dynamics, *J. Comput. Phys.*, 1995, **117**, 1–19.
30 A. Stukowski, Visualization and analysis of atomistic simulation data with OVITO–the Open Visualization Tool, *Modell. Simul. Mater. Sci. Eng.*, 2009, **18**, 015012.
31 O. Adjaoud and K. Albe, Microstructure formation of metallic nanoglasses: Insights from molecular dynamics simulations, *Acta Mater.*, 2018, **145**, 322–330.
32 O. Adjaoud and K. Albe, Influence of microstructural features on the plastic deformation behavior of metallic nanoglasses, *Acta Mater.*, 2019, **168**, 393–400.
33 O. Adjaoud and K. Albe, Nanoindentation of nanoglasses tested by molecular dynamics simulations: influence of structural relaxation and chemical segregation on the mechanical response, *Front. Mater.*, 2021, **8**, 664220.
34 M. Mendelev, M. Kramer, R. Ott, D. Sordelet, D. Yagodin and P. Popel, Development of suitable interatomic potentials for simulation of liquid and amorphous Cu–Zr alloys, *Philos. Mag.*, 2009, **89**, 967–987.
35 Y. Ritter, D. Şopu, H. Gleiter and K. Albe, Structure, stability and mechanical properties of internal interfaces in $Cu_{64}Zr_{36}$ nanoglasses studied by MD simulations, *Acta Mater.*, 2011, **59**, 6588–6593.
36 J. Zemp, M. Celino, B. Schönfeld and J. F. Löffler, Crystal-like rearrangements of icosa hedra in simulated copper–zirconium metallic glasses and their effect on mechanical properties, *Phys. Rev. Lett.*, 2015, **115**, 165501.

37 C. Kalcher, T. Brink, J. Rohrer, A. Stukowski and K. Albe, Interface-controlled creep in metallic glass composites, *Acta Mater.*, 2017, **141**, 251–260.
38 Y. Cheng, J. Ding and E. Ma, Local topology *vs*. atomic-level stresses as a measure of disorder: correlating structural indicators for metallic glasses, *Mater. Res. Lett.*, 2013, **1**, 3–12.
39 K. Zheng and P. S. Branicio, Synthesis of metallic glass nanoparticles by inert gas conden sation, *Phys. Rev. Mater.*, 2020, **4**, 076001.
40 J. Ding, Y.-Q. Cheng and E. Ma, Full icosahedra dominate local order in $Cu_{64}Zr_{34}$ metallic glass and supercooled liquid, *Acta Mater.*, 2014, **69**, 343–354.
41 R. Ranganathan, Y. Shi and P. Keblinski, Frequency-dependent mechanical damping in alloys, *Phys. Rev. B*, 2017, **95**, 214112.
42 H.-B. Yu and K. Samwer, Atomic mechanism of internal friction in a model metallic glass, *Phys. Rev. B: Condens. Matter Mater. Phys.*, 2014, **90**, 144201.
43 P. P. Singh and R. Ranganathan, Mechanical and viscoelastic properties of stackedv and grafted Graphene/Graphene oxide–polyethylene nanocomposites: a coarse-grained Molecular Dynamics Study, *ACS Omega*, 2024, **9**, 9063–9075.
44 D. J. Evans and G. Morriss, Nonlinear-response theory for steady planar Couette flow, *Phys. Rev. A*, 1984, **30**, 1528.
45 P. J. Daivis and B. Todd, A simple, direct derivation and proof of the validity of the SLLOD equations of motion for generalized homogeneous flows, *J. Chem. Phys.*, 2006, **124**, 194103.
46 A. P. Thompson, S. J. Plimpton and W. Mattson, General formulation of pressure and stress tensor for arbitrary many-body interaction potentials under periodic boundary conditions, *J. Chem. Phys.*, 2009, **131**, 154107.
47 J. Rieger, The glass transition temperature T_g of polymers—comparison of the values from differential thermal analysis (DTA, DSC) and dynamic mechanical measurements (torsion pendulum), *Polym. Test.*, 2001, **20**, 199–204.
48 J. Jiang, Z. Lu, J. Shen, T. Wada, H. Kato and M. Chen, Decoupling between calori metric and dynamical glass transitions in high-entropy metallic glasses, *Nat. Commun.*, 2021, **12**, 3843.
49 J. Ding, Y.-Q. Cheng, H. Sheng, M. Asta, R. O. Ritchie and E. Ma, Universal structural parameter to quantitatively predict metallic glass properties, *Nat. Commun.*, 2016, **7**, 13733.
50 R. Jana and L. Pastewka, Correlations of non-affine displacements in metallic glasses through the yield transition, *J. Phys.: Mater.*, 2019, **2**, 045006.
51 B. Fan and M. Li, Topology of icosahedral network responsible for yielding in CuZr metallic glasses, *Comput. Mater. Sci.*, 2024, **233**, 112682.
52 G.-J. Lyu, J.-C. Qiao, Y. Yao, Y.-J. Wang, J. Morthomas, C. Fusco and D. Rodney, Microstructural effects on the dynamical relaxation of glasses and glass composites: a molecular dynamics study, *Acta Mater.*, 2021, **220**, 117293.